

# Lawrence Berkeley National Laboratory

## Recent Work

### Title

Ultrafast dynamics in van der Waals heterostructures.

### Permalink

<https://escholarship.org/uc/item/8ct9t3nf>

### Journal

Nature nanotechnology, 13(11)

### ISSN

1748-3387

### Authors

Jin, Chenhao  
Ma, Eric Yue  
Karni, Ouri  
[et al.](#)

### Publication Date

2018-11-01

### DOI

10.1038/s41565-018-0298-5

Peer reviewed

---

# Ultrafast dynamics in van der Waals heterostructures

Chenhao Jin<sup>1</sup>, Eric Yue Ma<sup>2</sup>, Ouri Karni<sup>2</sup>, Emma C. Regan<sup>1,3,4</sup>, Feng Wang<sup>1,4,5\*</sup>, Tony F. Heinz<sup>2,6\*</sup>

<sup>1</sup> Department of Physics, University of California at Berkeley, Berkeley, California 94720, USA.

<sup>2</sup> Department of Applied Physics, Stanford University, Stanford, California 94305, USA.

<sup>3</sup> Graduate Group in Applied Science and Technology, University of California at Berkeley, Berkeley, California 94720, USA

<sup>4</sup> Material Science Division, Lawrence Berkeley National Laboratory, Berkeley, California 94720, USA.

<sup>5</sup> Kavli Energy NanoSciences Institute at University of California Berkeley and Lawrence Berkeley National Laboratory, Berkeley, California 94720, USA.

<sup>6</sup> SLAC National Accelerator Laboratory, 2575 Sand Hill Road, Menlo Park, California 94025, USA.

\* Correspondence to: [tony.heinz@stanford.edu](mailto:tony.heinz@stanford.edu), [fengwang76@berkeley.edu](mailto:fengwang76@berkeley.edu)

## Abstract

Van der Waals heterostructures are synthetic quantum materials composed of stacks of atomically thin two-dimensional (2D) layers. Because the electrons in the atomically thin 2D layers are exposed to layer-layer coupling, the properties of van der Waals heterostructures are defined not only by the constituent monolayers, but also by the interactions between the layers. Many fascinating electrical, optical, and magnetic properties have recently been reported in different types of van der Waals heterostructures. In this review we focus on unique excited-state dynamics in transition metal dichalcogenide (TMDC) heterostructures. TMDC monolayers are the most widely studied 2D semiconductors, featuring prominent exciton states and accessibility to the valley degree of freedom. Many TMDC heterostructures are characterized by a staggered band alignment. This band alignment has profound effects on the evolution of the excited states in heterostructures, including ultrafast charge transfer between the layers, the formation of interlayer excitons, and the existence of long-lived spin and valley polarization in resident carriers. Here we review recent experimental and theoretical efforts to elucidate electron dynamics in TMDC heterostructures, extending from time scales of femtoseconds to microseconds, and comment on the relevance of these effects for potential applications in optoelectronic and valleytronic/spintronic devices.

---

36 **Main text**

37 Advances in the isolation and manipulation of atomically-thin sheets of two-dimensional (2D) crystals,  
38 starting with the investigations of graphene a decade ago, have ushered in a new era of basic  
39 scientific research and technological innovation. 2D layers with diverse properties can now be  
40 prepared separately and then stacked together to form new types of quantum materials, known as  
41 van der Waals (vdW) heterostructures. The ability to combine materials with monolayer precision  
42 enables the design and creation of functional 2D materials that do not exist in nature. Today we have  
43 at our disposal a wide variety of atomically thin 2D layers, ranging from semiconducting MoS<sub>2</sub> and  
44 insulating hexagonal boron-nitride (h-BN) to magnetic CrI<sub>3</sub> and superconducting NbSe<sub>2</sub>, that can be  
45 stacked one upon the other. Since the electrons in atomically thin layers are exposed, different  
46 quantum states found in the individual layers can interact and couple to one another in ways that are  
47 not possible in other systems.

48  
49 VdW heterostructures constitute a vast family of new quantum materials, since they are defined not  
50 only by the combination of constituent monolayer materials, but also by the stacking sequence and  
51 relative crystallographic alignment of the layers. Further control of physical properties in 2D vdW  
52 heterostructures can be achieved through the application of electrostatic gating and fields, as well as  
53 substrate and strain engineering. Many fascinating physical phenomena have been reported in  
54 different vdW heterostructures, as exemplified by transport measurements revealing Hofstadter  
55 butterfly states, fractional Chern insulators, gate-tunable Mott insulators, unconventional  
56 superconductivity, etc<sup>1-7</sup>. In addition to electrical transport, there has also been great progress in the  
57 study of the optical properties and excited-state dynamics in vdW heterostructures. Here we review  
58 the new dynamical phenomena that emerge in semiconducting vdW heterostructures composed of  
59 stacked transition metal dichalcogenide (TMDC) layers. We focus our discussion on TMDC  
60 heterostructures, since the individual TMDC layers, with their many distinctive and intriguing  
61 properties, have already been well characterized and provide a strong basis for understanding the  
62 emergent new properties of heterostructures.

63  
64 TMDC semiconductors (MX<sub>2</sub> layers with 2H symmetry and M = Mo, W; X = S, Se, Te) exhibit direct  
65 gaps at monolayer thickness. They feature strong light-matter interactions and dramatically enhanced  
66 electron-electron interactions, with the optical properties largely defined by exciton states. The  
67 exciton binding energies in monolayer TMDCs are hundreds of meV— as much as two orders of  
68 magnitude larger than in typical bulk semiconductors like silicon or GaAs<sup>8,9</sup>. In addition, TMDC  
69 monolayers provide a platform to investigate and control the valley degree of freedom — often  
70 designated as valley pseudospin — associated with the energetically degenerate K and K' valleys and  
71 accessible optically through the presence of valley circular dichroism. The valley pseudospin in TMDC  
72 is, moreover, coupled to the electron/hole spin due to strong spin-orbit interactions<sup>10,11</sup>.

73  
74 Understanding the dynamic interplay and evolution of the charge, spin, and valley excitations in vdW  
75 heterostructures is of fundamental scientific interest. It is also of central importance for many potential  
76 applications of TMDC materials in optoelectronics, spintronics, and valleytronics. The dissociation of  
77 optically excited excitons into free carriers is, for example, critical for photovoltaic devices, while the  
78 ability to control and stabilize valley polarization is essential for valleytronic applications. The  
79 formation of vdW heterostructures in TMDC layers can profoundly affect their excited-state dynamics,  
80 ranging from the dissociation of intralayer excitons and the formation of interlayer excitons to the  
81 relaxation of spin and valley polarization. The use of vdW heterostructures provides a powerful  
82 platform to control and optimize the dynamic response of the constituent materials. In this review, we

83 survey recent progress in probing electron dynamics, extending from femtoseconds to microseconds,  
84 in TMDC heterostructures. On short time scales ( $\lesssim 1$ ps), the dynamics is dominated by the charge  
85 transfer and energy relaxation processes in the heterostructure. On longer time scales ( $\gtrsim 1$ ps), the  
86 recombination of interlayer excitons and relaxation of the spin and valley degrees of freedom become  
87 relevant. The rate of these processes can vary by orders of magnitude depending on the configuration,  
88 temperature, and doping of the heterostructure. We will also touch upon the dynamics of lateral  
89 transport of spin and valley polarization in TMDC heterostructures. We describe the physical  
90 mechanisms that underlie the different types of dynamic response in TMDC heterostructures and  
91 distinguish the behavior from that of the constituent layers, as well as mention briefly the implications  
92 for potential new technologies.

93

#### 94 **Band alignment in TMDC heterostructures**

95 In describing the single-particle electronic states in a vertical TMDC heterostructure, most authors in  
96 the literature consider the states to be largely localized within the individual layers. This approximation  
97 holds well for electronic states close to the band gap due to unusually weak interlayer coupling in  
98 TMDCs at the relevant K and K' points in the Brillouin zone (Fig. 1a)<sup>12</sup>. Therefore one can directly  
99 examine the relative energy difference, or band alignment, of material-specific electronic band  
100 extrema, just as is commonly done for heterostructures and quantum wells based on bulk  
101 materials<sup>13,14</sup>. An important distinction for atomically thin layers is that the concept of band bending  
102 near an interface does not apply<sup>15</sup>.

103

104 Semiconductor heterostructures can have different types of band alignment depending on the energy  
105 difference of the conduction and valence band extrema in the constituent layers (Fig. 1b)<sup>13,14</sup>. The  
106 lowest-lying states for electrons and holes reside in the same layer for a type-I heterostructure<sup>16</sup>, but  
107 are separated in different layers for a type-II heterostructure<sup>13,17</sup>. Further offsets in energy could, in  
108 principle, lower the conduction band minimum (CBM) of one layer to a position below the valence  
109 band maximum (VBM) of the other layer, yielding a type-III heterostructure<sup>18</sup>.

110

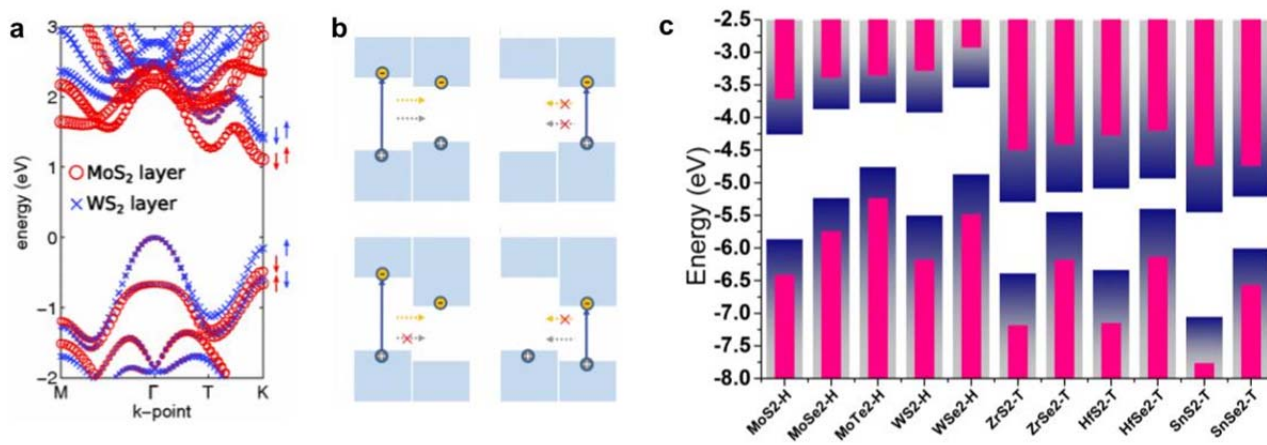
111 The type of band alignment has profound effects on the excited-state dynamics in a vdW  
112 heterostructure. In a type-I heterostructure carriers can only flow from the layer with the larger band  
113 gap to the layer with the smaller band gap (assuming that they do not have excess energy greater  
114 than the band offsets). The same applies to energy transfer through the exchange of virtual photons.  
115 In a type-II heterostructure, on the other hand, electrons accumulate in the layer with the lower CBM,  
116 while holes accumulate in the other layer<sup>17,19,20</sup>. Energy transfer can, however, still occur from the  
117 larger-gap to the smaller-gap material<sup>21</sup>.

118

119 There have been numerous theoretical studies of the band alignment in TMDC  
120 heterostructures<sup>13,14,18,22-24</sup>. The result of one recent calculation is shown in Fig. 1c. Many of the  
121 theoretical studies make use of DFT or related methods and cannot accurately account for the effects  
122 of doping (Fermi level difference), dielectric screening, and excitonic interactions<sup>25</sup>. They provide  
123 nonetheless guidelines for realizing specific types of heterostructures and combination of band gaps.  
124 Although theoretical studies are advancing rapidly, at present a definitive determination of  
125 heterostructure band alignment must rely on experiment<sup>26,27</sup>.

126

127 In the following, we describe experimental findings concerning the dynamics of charge and energy  
 128 transfer for representative TMDC heterostructures, followed by a summary of the relevant theoretical  
 129 studies.  
 130



131  
 132 **Fig. 1 Band alignment in vertical vdW heterostructures of TMDCs.** (a)  
 133 Calculated electronic states in a MoS<sub>2</sub>/WS<sub>2</sub> vertical heterostructure,  
 134 showing layer-localized states near the band edges at the K point<sup>12</sup>. (b)  
 135 Schematic of allowed charge transfer in heterostructures with type-I (top)  
 136 and type-II (bottom) band alignment<sup>16</sup>. (c) Calculated band-edge energies  
 137 for various TMDCs<sup>22</sup> based on different theoretical treatments: DFT-PBE  
 138 (blue) and G<sub>0</sub>W<sub>0</sub> (pink).

### 139 Charge transfer and energy transfer in TMDC heterostructures - Experiment

140 Following the predictions of type-II band alignment in TMDC heterostructures, several experimental  
 141 studies were reported that aimed (among other goals) to validate these theoretical results by probing  
 142 the associated charge transfer (CT) or energy transfer (ET) processes. Vertical heterostructures have  
 143 been examined for various material combinations prepared with different fabrication methods,  
 144 including stacking of layers exfoliated from bulk crystals and from layers grown by chemical vapor  
 145 deposition (CVD), as well as heterostructures grown directly by CVD.

146  
 147 Ultrafast optical measurements using pump-probe spectroscopy provide the possibility of accessing  
 148 charge and energy transfer processes with femtosecond (fs) time resolution. In initial experiments,  
 149 Hong *et al.* examined the dynamics of the MoS<sub>2</sub>/WS<sub>2</sub> heterostructure. Following excitation by an  
 150 ultrafast laser pulse resonant with the lower-energy MoS<sub>2</sub> A exciton, they observed a transient change  
 151 in reflectivity near the *higher-energy* WS<sub>2</sub> exciton (Fig. 2a)<sup>19</sup>. Based on theoretical predictions of type-  
 152 II band alignment of the two materials, this transient response was identified as arising from CT of a  
 153 hole from the MoS<sub>2</sub> monolayer to the WS<sub>2</sub> monolayer. By deconvolving the instrument response from  
 154 the rise-time of the signal, the authors were able to provide an upper limit of 50 fs for the charge  
 155 transfer time. Ceballos *et al.* observed similar dynamics in a heterostructure of MoS<sub>2</sub>/MoSe<sub>2</sub>, without  
 156 spectrally resolving the reflection of the probe<sup>28</sup>. They concluded, based on the theoretically predicted  
 157 band alignment, that electrons were transferred from MoSe<sub>2</sub> to MoS<sub>2</sub>. In addition, when exciting both  
 158 layers (using excitation resonant with the higher-energy exciton feature in MoS<sub>2</sub>) and comparing the

---

159 transient reflectivity signal of the monolayers to that of the heterostructure, the authors identified the  
160 presence of hole transfer in the opposite direction, *i.e.*, from MoS<sub>2</sub> to MoSe<sub>2</sub> (Fig. 2b).

161

162 Following these first experimental investigations, several groups examined the nature of the ultrafast  
163 CT for different types of heterostructures under different conditions. Heo *et al.* compared CVD-grown  
164 and manually stacked WS<sub>2</sub>/MoS<sub>2</sub> heterostructures with a focus on the dependence on the relative  
165 (twist) angle of the two constituent lattices<sup>29</sup>. Measuring the transient transmission of the probe signal,  
166 they did not resolve differences in the rise time of the signal associated with CT, but did observe a  
167 pronounced difference in the decay times of the signal. Wang *et al.* examined several WSe<sub>2</sub>/WS<sub>2</sub>  
168 heterostructures composed of CVD-grown layers mechanically stacked with different twist angles<sup>20,29</sup>.  
169 Using pump-probe measurements, together with steady-state techniques such as reflection contrast  
170 spectroscopy, they showed the same ultrafast signature from the onset of CT, either from electrons  
171 moving from WSe<sub>2</sub> to WS<sub>2</sub> or from holes traveling in the opposite direction. They concluded that  
172 interlayer CT takes place within 450 fs, close to the duration of the pump pulses in their experiment,  
173 and does not exhibit measurable sensitivity to the twist angle. Further reinforcing this conclusion, Zhu  
174 *et al.* explored deterministically aligned heterostructures of mechanically exfoliated MoS<sub>2</sub> and WSe<sub>2</sub>;  
175 they that the CT signal appears within 40 fs regardless of twist angle (Fig. 2c)<sup>30</sup>. On the other hand,  
176 the time scale of the decay was varied with the twist angle, but without any clear trend. Ji *et al.*  
177 reported a similar CT rise time for stacks of CVD-grown MoS<sub>2</sub> and WS<sub>2</sub> (Ref<sup>31</sup>). Such rapid interlayer  
178 CT irrespective of crystal orientation (and thus crystal momentum) is somewhat unintuitive. Chen *et*  
179 *al.* probed intraband transitions in a heterostructure using infrared light and suggested a potential  
180 explanation based on the rapid formation of “hot” interlayer excitons<sup>32</sup>. Additional theoretical  
181 investigations are summarized in the next section.

182

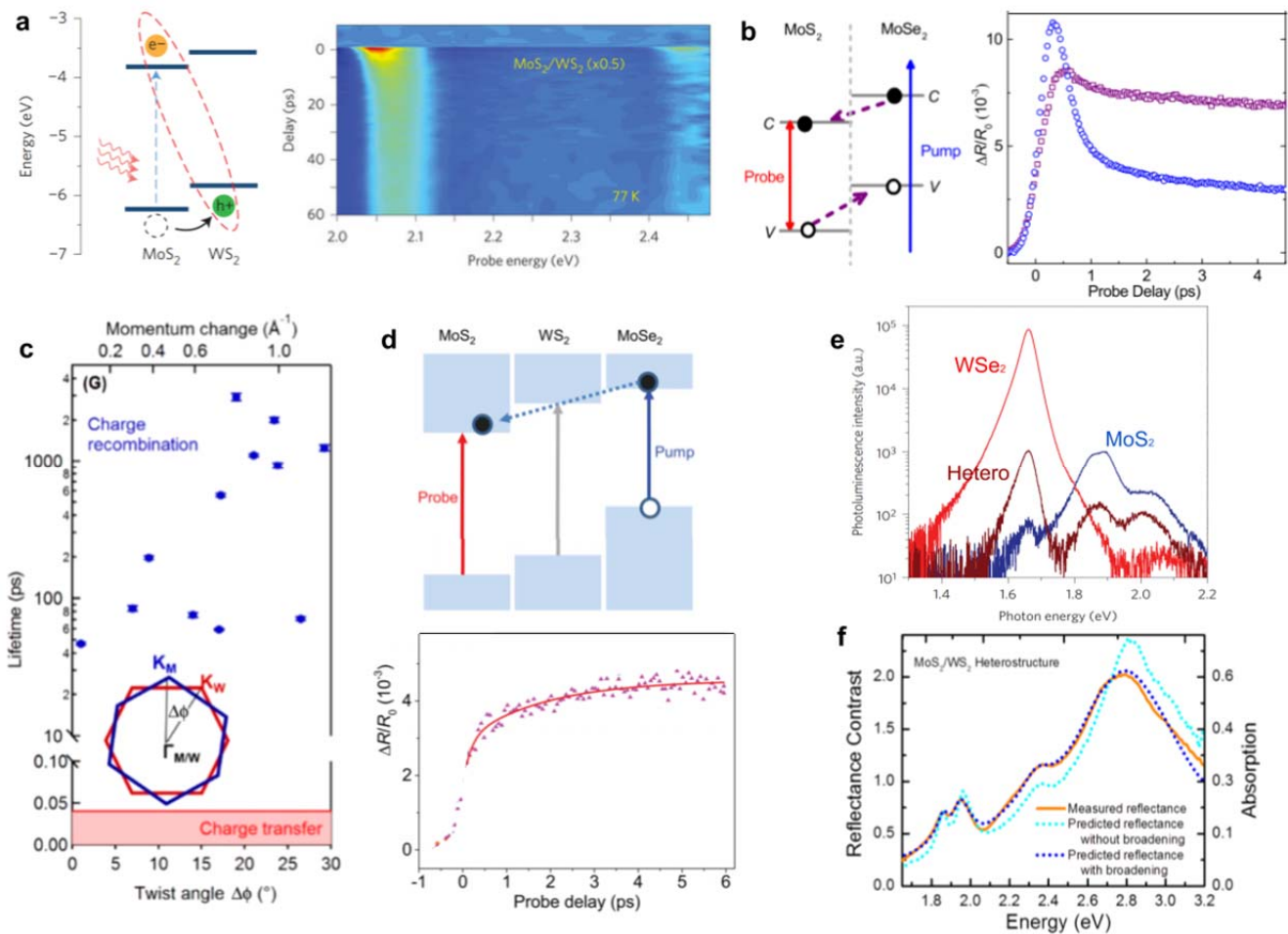


**Fig. 2 Experimental studies of ultrafast charge transfer in vertical TMDC heterostructures.** (a) Schematic and energy-resolved transient absorption spectra of a MoS<sub>2</sub>/WS<sub>2</sub> heterostructure, excited by an optical pulse near the lower-energy MoS<sub>2</sub> A exciton feature, indicating hole transfer<sup>19</sup>. (b) Schematic and time-resolved differential reflection of a MoS<sub>2</sub>/MoSe<sub>2</sub> heterostructure (blue) and of monolayer MoS<sub>2</sub> (purple), excited by an optical pulse above the band gaps of both materials, indicating both electron and hole transfer<sup>28</sup>. (c) Charge transfer (red shading) and recombination (blue) times in heterostructures of MoS<sub>2</sub> and WSe<sub>2</sub> with different twist angles, as indicated<sup>30</sup>. (d) Differential reflection at the energy of the MoS<sub>2</sub> A exciton following excitation at the energy of the MoSe<sub>2</sub> A exciton in a MoSe<sub>2</sub>/WS<sub>2</sub>/MoS<sub>2</sub> trilayer heterostructure<sup>33</sup>. (e) PL quenching<sup>34</sup> in MoS<sub>2</sub>/WSe<sub>2</sub> and (f) broadening of the features absorption features<sup>35</sup> in a MoS<sub>2</sub>/WS<sub>2</sub> heterostructure compared to the response of the separated monolayers.

183  
184  
185  
186  
187  
188  
189  
190  
191  
192  
193  
194  
195  
196  
197  
198  
199  
200  
201  
202  
203  
204

Further demonstrating its robustness, the signature of ~ps electron transfer was observed in a trilayer heterostructure where monolayers of MoSe<sub>2</sub> and MoS<sub>2</sub> were separated by a monolayer WS<sub>2</sub> (Fig. 2d, Ref.<sup>33</sup>). The authors suggested that such rapid CT across multiple materials is coherent, rather than sequential.

205 CT dynamics was also revealed in investigations of the coupling between pairs of TMDC layers. CT in  
206 a MoS<sub>2</sub>/MoTe<sub>2</sub> heterostructure was identified using pump-probe experiments<sup>36</sup>, leading to the  
207 suggestion of MoTe<sub>2</sub> as a good electrical contact for other semiconducting TMDCs and metals. Later,  
208 cascaded transfer of electrons and holes across several TMDCs heterostructures was invoked to  
209 explain correlated blinking observed in the photoluminescence (PL) in those stacks<sup>37</sup>.

210  
211 In addition to these time-resolved pump-probe measurements, CT between two TMDC layers in a  
212 heterostructure has been inferred from quenching of the photoluminescence of the constituent  
213 monolayers<sup>19,20,28-33,38-40</sup> and by broadening of the resonant features in the monolayers in optical  
214 absorption measurements<sup>20,35</sup>, both phenomena arising as a consequence of the presence of  
215 additional relaxation channels in the heterostructures. A reduction in the PL intensity by factor of a few  
216 tens to a few hundreds has commonly been observed (Fig. 2e)<sup>19,34</sup>. This suggests a corresponding  
217 ratio for the charge transfer time compared to the population lifetime in the isolated material.  
218 Assuming the latter to be a few hundred picoseconds for excitons in monolayer TMDCs<sup>41</sup> at room  
219 temperature, we estimate a CT time of ~1 ps, somewhat longer than measured by pump-probe  
220 techniques. This discrepancy can be explained as the result of a small fraction of the heterostructure  
221 exhibiting poor contact between the layers, thus yielding reduced PL quenching compared to that of  
222 the ideal structure. In optical absorption measurements, linewidth broadening of heterostructures  
223 compared with that of the separate monolayers has been reported and used to estimate non-radiative  
224 decay rates comparable to those deduced from pump-probe experiments (Fig. 2f)<sup>35</sup>. Extrinsic factors,  
225 such as strain introduced in fabricating the heterostructure, can potentially also play a role. The  
226 extremely rapid (few femtosecond) relaxation times inferred for high-lying states may, however,  
227 remain difficult to probe directly in the time domain, but is easily observable by lineshape analysis.

228  
229 Another dynamic process that may compete with CT is energy transfer (ET). In this latter process, an  
230 exciton created in one layer recombines, and the released energy creates an exciton in the other layer.  
231 Kozawa *et al.* reported evidence for such a process in a MoSe<sub>2</sub>/WS<sub>2</sub> heterostructure (Ref<sup>21</sup>) on the  
232 basis of a measured enhancement of PL from the MoSe<sub>2</sub> feature under excitation resonant with the  
233 WS<sub>2</sub> optical band gap. Recently, ET was also identified in heterostructures of MoS<sub>2</sub> and WS<sub>2</sub>  
234 separated by insulating layers of h-BN<sup>42</sup>. In these structures, PL quenching from the heterostructure  
235 was reduced, or even become PL enhancement, upon increasing the thickness of the h-BN spacer.  
236 This was interpreted as an ET process between B excitons in MoS<sub>2</sub> and A excitons in WS<sub>2</sub>. The  
237 dependence of the enhancement on spacer thickness, with an optimum of PL enhancement for ~5  
238 layers of h-BN and subsequent reduction of this effect with increasing layer thickness, is compatible  
239 with the predicted trend for a dipole-dipole interaction. This highlights the major difference between  
240 ET and CT processes: While the latter requires intimate coupling of the two constituent monolayers,  
241 the former, originating in dipole-dipole interactions, can act at greater distances and across insulating  
242 spacers. Although this difference between the processes is clear, there is currently little direct  
243 experimental information on the absolute rates of energy transfer for TMDC layers and in what  
244 regimes and under what conditions energy transfer competes with charge transfer.

## 245 **Charge transfer and energy transfer in TMDC heterostructures – Interpretation and theory**

246 Since most experiments have excited and probed excitonic resonances of the constituent layers, it  
247 has often been assumed that CT occurs between their direct band-edge (K/K' valley) states. Band  
248 structure calculations have shown that the K/K' states are localized around the central layer of metal  
249 atoms and have weak interlayer interactions. On the other hand, for states of different momentum,



250 such as in the  $\Gamma$  or Q valleys, the interlayer coupling may be significantly stronger. One consequence  
251 of this difference is the transition from indirect to direct band gap upon thinning TMDCs to the  
252 monolayer limit: the bulk CBM in the Q valley, more affected by interlayer coupling, lies above the K  
253 valley in monolayers<sup>43,44</sup>. For the same reason, the K-valley states are not expected to show such  
254 rapid interlayer charge transfer. This contradiction with experiment is further heightened by the  
255 apparent independence of CT on twist angle and lattice mismatch, the factors that dictate the  
256 momentum difference between the initial and final states, as well as its insensitivity to temperature.  
257 Here we briefly survey some of the approaches presented in the literature to identify the mechanism  
258 responsible for the very efficient CT processes observed experimentally in vertical TMDC  
259 heterostructures.

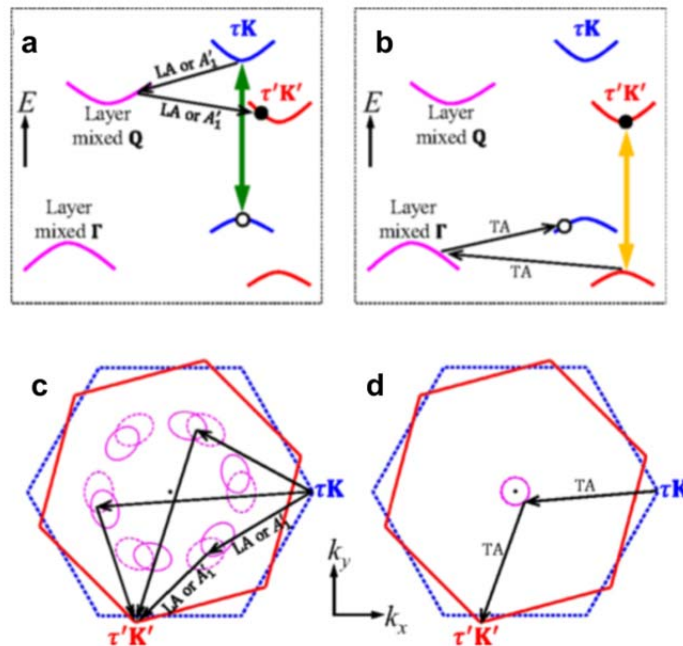
260  
261 Zhu *et al.*, following considerations relevant for CT processes in molecular systems, have pointed out  
262 the possible role of localization in bridging the momentum mismatch<sup>45</sup>. The electrostatic attraction  
263 between the optically excited electron and hole, which leads to the formation of tightly bound excitons,  
264 gives rise to a distribution of momenta for the charge carriers across a significant range wavevectors  
265 in the Brillouin zone (BZ). This situation could explain the apparent lack of momentum conservation in  
266 the observed CT process. However, it is unclear with this effect alone could supply the large  
267 momentum required for CT in heterostructures with large twist angles<sup>30</sup>. In addition, for excitation  
268 substantially above the band gap, it is unclear whether exciton formation occurs prior to charge  
269 transfer<sup>28</sup>.

270  
271 Several groups have also employed numerical calculations using molecular dynamics (MD) and time-  
272 dependent density-functional theory (TD-DFT) to elucidate the mechanism for interlayer charge  
273 transfer. Since accurately accounting for the effect of excitons is computationally demanding, these  
274 calculations have focused on the transfer of free charge carriers from one monolayer to its neighbor.  
275 Wang *et al.* described a process of transferring holes directly between the K valleys of the two layers  
276 mediated by the electric dipole interaction of the initial and final states, which enhances the coupling  
277 between the states to above a critical level for collective charge transfer<sup>46</sup>. In this description, both  
278 twist angle and temperature have a significant influence on the transfer rate<sup>46</sup>. Zhang *et al.* pointed  
279 out the significance of such dipole coupling between specific states in the vicinity of the K valley and  
280 highlighted the expected twist-angle dependence of the CT rate<sup>47</sup>. Additionally, the authors argue that  
281 the omission of excitonic effects for above gap excitation may not be significant if the time scales for  
282 CT and exciton formation are comparable. (This argument is, however, problematic for explaining CT  
283 from excitons created directly by resonant excitation.)

284  
285 A slightly different picture is presented by Long *et al.*<sup>48</sup> and by Li *et al.*<sup>49</sup> for CT processes in  
286 MoSe<sub>2</sub>/MoS<sub>2</sub> and MoS<sub>2</sub>/WS<sub>2</sub> systems, respectively. They propose that holes and/or electrons undergo  
287 transfer from one layer to the other due to mixing between the electronic states near the K point of  
288 both layers<sup>48,49</sup>: the states into which the charge carriers are optically injected are coherently mixed  
289 (and therefore delocalized) across the two layers, so that CT need only to be driven by an intralayer  
290 relaxation process to the K-valley, mediated by phonon emission. In this model, the coupling relies on  
291 specific layer orientations to facilitate the state mixing in the heterostructure. The discrepancy  
292 between this requirement and the apparent twist-angle independence of CT in experiments is  
293 explained in terms of changes in the relative local atomic positions in the two layers across the moiré  
294 pattern of the heterostructure<sup>50,51</sup>. Regardless of the twist angle of the layers, such lateral  
295 inhomogeneity provides regions where the coupling between the layers is strong<sup>31</sup>. In all of the above  
296 scenarios, phonons are necessary for the completion of the CT process, but not for its initiation.

297  
298  
299  
300  
301  
302  
303  
304  
305  
306  
307  
308  
309  
310  
311  
312

Recent work has also explored a more direct role for phonons in the initiation of CT. Wang *et al.* considered momentum-conserving charge transfer between the layers in various regions of the BZ, including at the K, Q and  $\Gamma$  points for different twist angles and degrees of lattice mismatch<sup>52</sup>, as shown in Fig. 3a-d. The proposed mechanism involves scattering by phonons from the K valley to the  $\Gamma$  valley (for holes) or to the Q valley (for electrons), regions where the interlayer coupling is strong and interlayer charge transfer is rapid. After charge transfer, scattering with another phonon would bring the charge carriers back to the K-valley. For intralayer scattering within 20 fs, the entire charge transfer process would occur in less than 100 fs, as observed experimentally. A similar scheme was developed by Zheng *et al.* using a numerical MD TD-DFT calculation, although without accounting for inhomogeneities from the moiré pattern<sup>53</sup>. These theories better match the observed twist-angle independence, as the coupling around the  $\Gamma$  and Q points is not sensitive to the layer orientation. The expected temperature dependence of this mechanism is also weak, as it only requires emission of phonons to dissipate the excess energy available from the transfer. This general mechanism has been adopted in the interpretation of recent experiments related to CT processes<sup>30,33,39</sup>.



313  
314  
315  
316  
317  
318  
319  
320  
321  
322  
323

**Fig. 3 Theoretical concepts explaining the robust and ultrafast nature of CT in TMDC heterostructures<sup>52</sup>.** (a) Schematic representation of phonon mediated electron transfer. (b) The same for hole transfer. (c) Top view of the twisted BZ of the two layers, where electron transfer between the K-points is mediated by phonon coupling to the Q-point. (d) The same for hole transfer, mediated in this case by the coupling to the  $\Gamma$ -point.

---

## 324 **Spin and valley dynamics in TMDC heterostructures**

325 The previous sections addressed carrier dynamics in TMDC heterostructures on the ultrafast time  
326 scale ( $\lesssim 1$ ps) relevant for interlayer charge transfer in systems with type-II band alignment. In the  
327 following section, we focus on spin and valley relaxation dynamics in TMDC heterostructures, which  
328 take place on considerably longer time scales.

329  
330 Within a TMDC monolayer, there are two distinct relaxation processes to consider. First, the  
331 population decay of optically excited excitons has a characteristic time scale of few picoseconds to  
332 nanoseconds, depending on choice of material, sample preparation, temperature, etc.<sup>54-58</sup>. Second,  
333 the exciton spin-valley lifetime, which determines how long information can be stored in the spin-  
334 valley degree of freedom, has been found to be a few picoseconds in isolated monolayer TMDCs<sup>59-63</sup>.  
335 Both the population and the spin-valley lifetimes in type-II heterostructures, where the electrons and  
336 holes reside in different layers after the rapid initial charge transfer process, can differ markedly from  
337 the corresponding lifetimes in isolated monolayers.

338  
339 Below we review recent experimental results on dynamics on the pico-to-micro-second time scale in  
340 heterostructures and show that both the population lifetime and the spin-valley lifetime can be  
341 significantly longer than for the monolayer case. We then summarize recent efforts towards  
342 understanding the physical mechanisms of the corresponding intervalley scattering processes. Finally,  
343 we discuss the spatio-temporal dynamics of spin and valley polarization in TMDC heterostructures.  
344

## 345 **Long spin and valley lifetime in TMDC heterostructures**

346 Traditional electronic devices are based on the manipulation of electron charges in the real space.  
347 Using other electron degrees of freedom as the information carrier, such as spin and valley, can  
348 potentially overcome fundamental limits of speed and power consumption, giving rise to intriguing new  
349 concepts in spintronics and valleytronics. A long spin/valley lifetime is necessary to ensure that the  
350 spin/valley information will be maintained in the idle state and can persist long enough to be  
351 processed. We note that the valley lifetime discussed here should not be confused with the valley  
352 depolarization time: the former can originate from different mechanisms, including the population  
353 decay of the valley information carriers, while the latter only describes the intervalley scattering  
354 process.

355  
356 TMDCs offer a promising platform for spintronic and valleytronic applications, owing to several  
357 attractive properties of these materials. The valley-dependent optical selection rule allows for  
358 convenient creation, manipulation, and detection of excitons in specific valleys with circularly polarized  
359 light<sup>64-66</sup>. Furthermore, the spin-valley locking effect suggests that a very long spin-valley lifetime is  
360 possible because intervalley scattering of electrons or holes requires both a large momentum change  
361 from K to K' and a simultaneous spin flip<sup>10,11</sup>. However, several groups have measured exciton spin-  
362 valley dynamics using time-resolved Kerr rotation (TRKR)<sup>59-63</sup>, and the spin-valley lifetime was found  
363 to be rather short, ranging from one to few picoseconds, even at low temperatures. This counter-  
364 intuitive observation was later explained as a consequence of the exchange interaction between  
365 excitons in the two valleys<sup>67-70</sup>: a bright exciton always has total momentum and spin of zero and  
366 therefore does not require any change in momentum or spin to scatter to the other valley as an intact  
367 exciton. This reduced spin-valley lifetime of excitons in TMDC monolayers significantly limits their use  
368 in carrying spin-valley information.

369

370 A general strategy for improving the spin-valley lifetime in TMDCs is to eliminate the exciton exchange  
371 interaction by converting excitons into other excitations that serve as alternative carriers of valley  
372 information. An additional figure of merit, the conversion efficiency, must be introduced to quantify the  
373 final valley imbalance created from each optically excited exciton. To avoid loss of valley information  
374 during conversion, the time scale of the conversion process (*i.e.*, the exciton population lifetime) must  
375 be comparable to or shorter than the picosecond spin-valley lifetime of excitons. In monolayer TMDCs,  
376 several candidates have been considered as the alternative information carriers, including trions<sup>71-73</sup>,  
377 dark excitons<sup>74,75</sup>, biexcitons<sup>76,77</sup>, and resident carriers<sup>78-81</sup>. For example, Fig. 4a,b show the valley  
378 dynamics of trions and resident electrons probed by TRKR measurement. Unlike bright excitons,  
379 these excitations have non-zero total momentum and/or total spin, and therefore will not suffer from  
380 rapid spin-valley relaxation through the exchange interaction. Their spin-valley lifetimes at low  
381 temperatures range from tens of picoseconds to a microseconds, but the conversion efficiency from  
382 the initially generated exciton has rarely been characterized. However, since the exciton population  
383 lifetime is comparable to or longer than the exciton spin-valley lifetime in these cases, the valley  
384 conversion efficiency is likely to be considerably less than unity.

385

386 On the other hand, the interlayer charge transfer process in type-II heterostructures provides an  
387 attractive mechanism to break intralayer excitons on the femtosecond time scale. As discussed above,  
388 the ultrafast charge transfer process occurs very rapidly, typically within ~50 fs, in TMDC  
389 heterostructures<sup>19,82</sup>. Because this time scale is much faster than exciton spin-valley relaxation, the  
390 loss of spin-valley information during the conversion process is expected to be minor.

391

392 In nearly aligned heterobilayers, electrons and holes can form bright interlayer excitons after the  
393 charge transfer process<sup>28,40,83</sup>. Rivera *et al.* observed 40% positive circular helicity from interlayer  
394 exciton emission in WSe<sub>2</sub>/MoSe<sub>2</sub> bilayer and measured a spin-valley lifetime of a few nanoseconds in  
395 a time-resolved photoluminescence (TR-PL) study<sup>84</sup>, as shown in Fig. 4c. The significantly longer  
396 spin-valley lifetime of interlayer excitons can be understood by noting that the electron and hole  
397 wavefunctions have much smaller overlap in interlayer excitons compared to intralayer excitons; they  
398 will therefore have a weaker exchange interaction and exhibit slower recombination processes (both  
399 radiative and non-radiative).

400

401 Recently, there has been increasing research interest in the nature of the interlayer exciton state and  
402 the origin of the circular helicity of emission in nearly aligned heterostructures. Hsu *et al.* reported  
403 negative circular helicity of interlayer exciton emission<sup>85</sup> in WSe<sub>2</sub>/MoSe<sub>2</sub> bilayer, while Ciarrocchi *et al.*  
404 and Hanbicki *et al.* observed two separate interlayer exciton emission peaks with opposite signs of  
405 helicity<sup>86,87</sup>. Meanwhile, various configurations of interlayer excitons have been proposed as the  
406 emitting state, including spin singlet zero-momentum excitons<sup>84,88</sup>, spin-triplet zero-momentum  
407 excitons<sup>89</sup>, and finite-momentum excitons<sup>90,91</sup>. The rich set of observations originates in part from the  
408 complex conduction band structure in the WSe<sub>2</sub>/MoSe<sub>2</sub> bilayer, where electron states of spin up and  
409 spin down, and at K and Q valleys, are all close in energy. Furthermore, the real-space distribution of  
410 interlayer excitons when a moiré pattern is present can further modify the optical selection rules<sup>92,93</sup>.  
411 The exact mechanisms behind these interesting observations are yet to be fully understood.

412

413 An alternative approach involves using single-particle states, such as holes in WSe<sub>2</sub> to carry valley  
414 information in the heterostructure. Because the momentum match between electrons and holes  
415 (required for efficient exciton emission) is not relevant in this approach, a large-twist-angle bilayer is

416 preferred to separate electrons and holes in momentum space and further reduce their exchange  
417 interaction and recombination rate. Kim *et al.* measured the spin-valley lifetime of holes in  
418 WSe<sub>2</sub>/MoS<sub>2</sub> heterostructures using circularly polarized pump-probe spectroscopy<sup>94</sup>. Figure 4d shows  
419 the measured decay dynamics of the total hole population and valley-polarized hole population in the  
420 WSe<sub>2</sub> layer at a temperature of 10 K. Both the population lifetime and the spin-valley lifetime of holes  
421 are around one microsecond, indicating that the decay of the spin-valley imbalance occurs primarily  
422 through population loss. On the other hand, the valley polarization remains almost a constant for a  
423 few microseconds, from which one can extract a valley depolarization time (or intervalley scattering  
424 time) exceeding 40 μs. The other critical figure of merit, the conversion efficiency, was also  
425 determined experimentally to be close to unity for valley-polarized holes<sup>94</sup>. The nearly ideal  
426 conversion efficiency is consistent with an interlayer charge transfer process that is far faster than  
427 intervalley scattering processes.

428  
429 The spin-valley lifetime of resident holes in the heterostructure can be further improved by tuning the  
430 carrier concentration. Figure 4e summarizes the doping-dependent spin-valley lifetime of holes in a  
431 WSe<sub>2</sub>/WS<sub>2</sub> heterostructure (red circles), as compared to the population lifetime of holes (blue  
432 triangles)<sup>95</sup>. In charge neutral and electron-doped heterostructures, the spin-valley lifetime is similar to  
433 the population lifetime; however, for hole-doping, the spin-valley lifetime becomes orders of  
434 magnitude longer than the population lifetime. This doping dependence is a consequence of the  
435 interlayer electron-hole recombination process, as shown in Fig. 4f,g. For electron-doped or charge  
436 neutral heterostructures (Fig. 4f), all of the holes in WSe<sub>2</sub> are pump-generated excess holes.  
437 Therefore, when hole population decays to zero due to interlayer electron-hole recombination, no  
438 holes -- and certainly no valley-polarized holes -- remain in the WSe<sub>2</sub>. The valley lifetime is then  
439 limited by the lifetime of the total hole excess. On the other hand, if the original hole density is much  
440 greater than the photo-generated density, excess electrons in WS<sub>2</sub> will recombine with holes from  
441 both valleys of WSe<sub>2</sub> with nearly equal probability (Fig. 4g). Consequently, a pure spin-valley  
442 imbalance (*i.e.*, equal excess and deficiency of holes in the K and K' valley) is generated, the lifetime  
443 of which can be much longer than the population lifetime and has been found to exceed 20 μs.  
444 Furthermore, the decrease of spin-valley imbalance is negligible during the population decay, and the  
445 overall efficiency of this two-step conversion process can approach 100%<sup>95</sup>.

446  
447  
448  
449

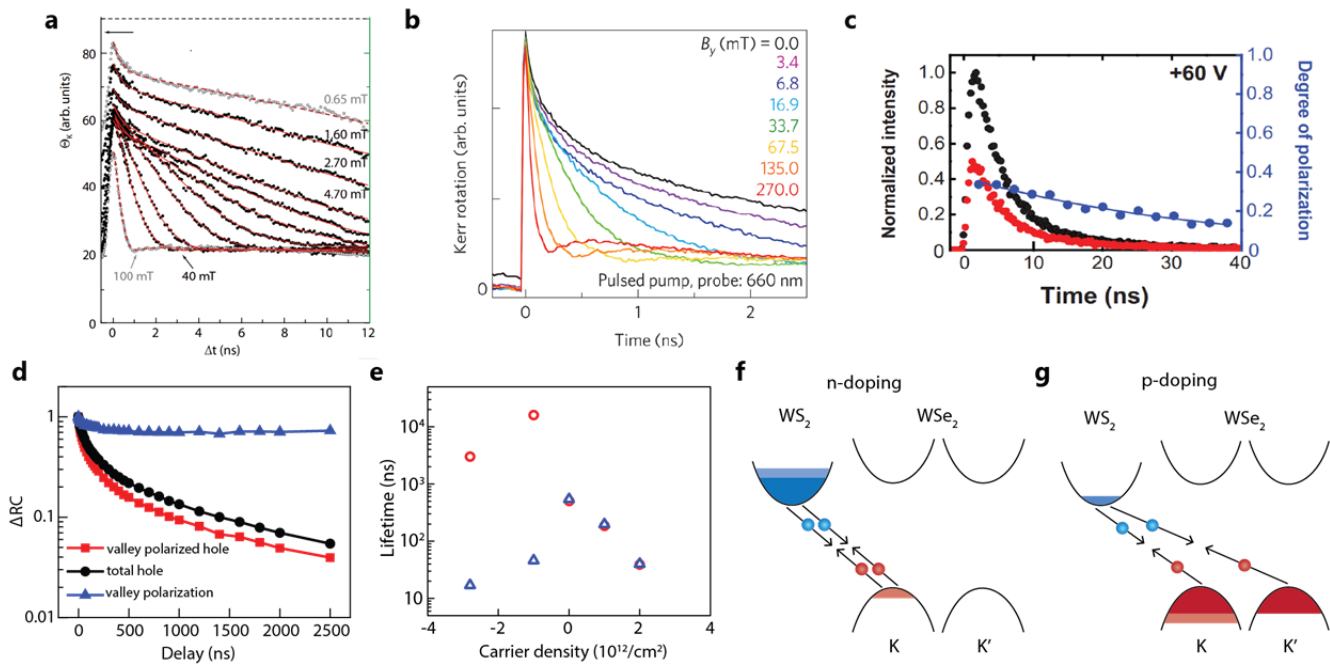


Fig. 4 Dynamics of spin-valley information carriers in TMDC

materials. (a-b) Spin-valley dynamics of trions (a)<sup>72</sup> and resident electrons (b)<sup>81</sup> in monolayer TMDC materials under different external magnetic fields as probed by time-resolved Kerr rotation measurements.

A spin-valley lifetime of few to tens of nanoseconds is observed at low fields. (c) Time-resolved photoluminescence in a nearly aligned WSe<sub>2</sub>/MoSe<sub>2</sub> heterobilayer for the same (black) and opposite (red) circularly polarized excitation, revealing a valley lifetime of few nanoseconds<sup>84</sup>.

(d) Decay dynamics of the valley-polarized hole population, the total hole population, and the valley polarization in a large-twist-angle WSe<sub>2</sub>/MoS<sub>2</sub> heterostructure at charge neutrality<sup>94</sup>.

(e) Summary of the hole population (blue) and spin-valley (red) lifetimes as a function of carrier concentration in a large-twist-angle WSe<sub>2</sub>/WS<sub>2</sub> heterostructure<sup>95</sup>.

(f-g) Schematic illustration of the interlayer electron-hole recombination process in electron-doped (f) and hole-doped (g) heterostructures.

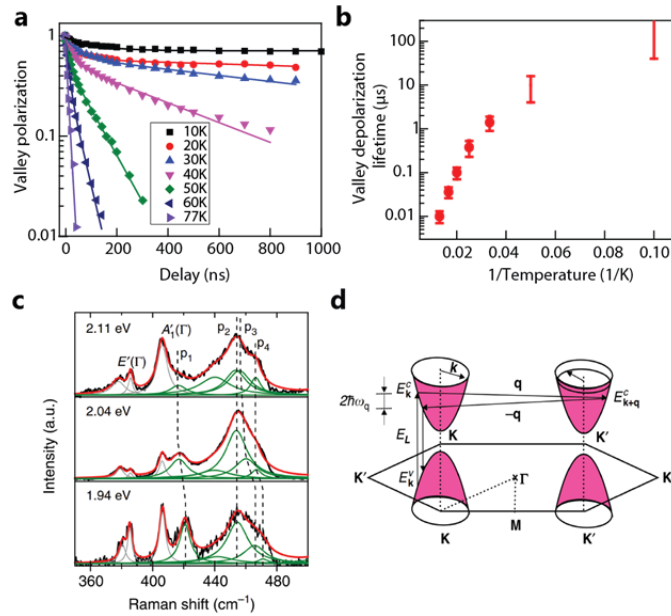
450  
451  
452  
453  
454  
455  
456  
457  
458  
459  
460  
461  
462  
463  
464  
465  
466  
467  
468

### Potential mechanism behind intervalley scattering

As discussed in the previous sections, the spin-valley lifetime can be limited either by the population lifetime or by the intervalley scattering process. The first limitation can be removed for valley-polarized holes in hole-doped heterostructures, making them promising candidates for spin-valley information carriers. Furthermore, directly probing hole dynamics provides relatively clean information about the decay mechanism owing to the simplicity of the valence band maximum. This configuration thus provides a valuable platform for understanding intervalley scattering processes in TMDC materials.

477 Figure 5a shows the decay dynamics of valley polarization at different temperature for holes in  
478 WSe<sub>2</sub>/MoS<sub>2</sub> heterostructures, with the valley depolarization lifetime summarized in Fig. 5b (Ref. <sup>94</sup>).

479 The depolarization lifetime changes from 10 ns at 77 K to above 40  $\mu$ s at 10 K, which roughly follows  
 480 a thermally activated rate:  $\tau \sim \exp\left(\frac{\Delta}{k_B T}\right)$ , with  $k_B$  denoting the Boltzmann constant and  $\Delta \sim 20$  meV.  
 481  
 482



483  
 484 **Fig. 5 Potential origin of intervalley scattering in WSe<sub>2</sub>/MoS<sub>2</sub>**  
 485 heterostructures. (a) Temperature-dependent decay dynamics of valley  
 486 polarization. (b) Temperature dependence of the intervalley scattering  
 487 time. The process can be described as thermally activated<sup>94</sup>. (c)  
 488 Resonant Raman spectra of single-layer MoS<sub>2</sub> show particularly strong  
 489 second-order Raman signals (peaks p1 to p4) for excitation around 2.0  
 490 eV through a doubly resonant Raman (DRR) process involving K point  
 491 phonons, as illustrated in (d)<sup>96</sup>.  
 492

493 The inter-valley scattering of holes in WSe<sub>2</sub> requires a large momentum change and a simultaneous  
 494 spin flip. However, due to the strong spin-orbit coupling in WSe<sub>2</sub>, the picture of electrons and holes  
 495 with perfectly defined up and down spin states in the K and K' valleys, respectively, is not strictly valid  
 496 for states away from the K and K' points. Therefore, inter-valley scattering of carriers near, but not  
 497 exactly at K and K' points is allowed. This process, often designated as the Elliott-Yafet mechanism,  
 498 has a characteristic temperature dependence of

$$\tau_{EY}^{-1} \sim T^2 \tau_p^{-1},$$

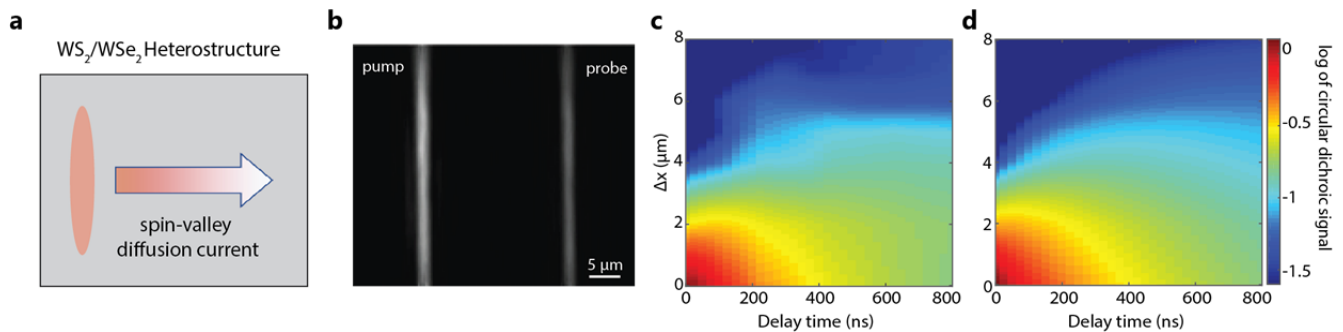
499 where  $\tau_p$  is the momentum scattering lifetime for a spin-conserving process. The  $T^2$ -dependence  
 500 originates from the fact that at higher temperature, thermally excited carriers are further away from  
 501 band minima (K or K') and will therefore scatter more efficiently. However, the predicted  $T^2$   
 502 dependence does not describe the strong observed variation with temperature, which presumably  
 503 reflects from the temperature dependence of  $\tau_p^{-1}$ . Indeed, a thermally activated temperature  
 504 dependence is expected for phonon-assisted intervalley scattering at low temperatures, and the  
 505 experimental activation energy of  $\sim 20$  meV agrees with WSe<sub>2</sub> phonon energy (at the K-point) required  
 506 for intervalley scattering<sup>96</sup>. Phonon-assisted intervalley scattering, accompanied by spin flip through  
 507 the Elliott-Yafet mechanism, can thus account for the observed spin-valley depolarization of holes.  
 508



509 The important role of K-point phonons in intervalley scattering is also supported by a recent resonant  
 510 Raman study<sup>96</sup>, which reveals second-order Raman signals (peaks p1 to p4 in Fig. 5c) assigned to K-  
 511 point phonons through a doubly resonant Raman (DRR) scattering process. This observation  
 512 suggests a strong interaction between charge carriers and K-point phonons, which dramatically  
 513 enhances their second-order Raman signals through the DRR process illustrated in Fig. 5d.  
 514

## 515 Spin-valley transport in TMDC heterostructures

516 The efficient generation of pure spin-valley imbalance in hole-doped WSe<sub>2</sub>/WS<sub>2</sub> heterostructures  
 517 provides a convenient way to create pure spin-valley current (Fig. 6a), which lies in the heart of spin-  
 518 valley-tronic devices. Jin *et al.* performed space-and-time-resolved pump-probe spectroscopy to track  
 519 the evolution of the spin-valley imbalance and to image the flow of pure spin-valley diffusion currents  
 520 (Fig. 6b). Figure 6c shows experimental results for a hole-doped WS<sub>2</sub>/WSe<sub>2</sub> heterostructure at an  
 521 initial electrostatic hole doping of  $p_0 = 1 \times 10^{12} / \text{cm}^2$ . At zero time delay, the spin-valley imbalance  
 522 matches the pump beam spatial profile (half-width of  $\sim 1.5 \mu\text{m}$ ); the signal is negligible for a pump-  
 523 probe separations greater than  $3 \mu\text{m}$ , as expected based on the convolution with probe spatial profile.  
 524 At finite delay time, the spin-valley imbalance diffuses out of the excitation region, generating a pure  
 525 spin-valley current. This leads to a strong decrease and increase of signal, respectively, in regions  
 526 near and far away from the pump beam. The spin-valley current propagates to distances over  $8 \mu\text{m}$   
 527 within 800 ns. Such direct imaging of the experimental spin-valley current flow (Fig. 6c) allows us to  
 528 determine important physical parameters by comparison with a diffusion-decay model (Fig. 6d). We  
 529 infer a diffusion constant of  $D = 0.2 \text{ cm}^2/\text{s}$ , a spin-valley lifetime of  $\tau = 20 \mu\text{s}$ , and deduce a spin-valley  
 530 diffusion length of  $l = \sqrt{D\tau} = 20 \mu\text{m}$ .  
 531



532  
 533  
 534 Fig. 6 **Spin-valley transport in a vdW heterostructure**<sup>95</sup>. (a) Optical  
 535 excitation of pure spin-valley imbalance at the left edge of a device will  
 536 create a pure spin-valley diffusion current flowing to the right without any  
 537 associated charge current. (b) Experimental configuration for direct  
 538 imaging of the spin-valley current flow with space-and-time resolved  
 539 pump-probe spectroscopy using pump and probe beams focused to lines  
 540 on the sample at defined spatial separation. (c-d) Experimentally  
 541 measured spatio-temporal evolution of the pure valley imbalance in the  
 542 heterostructure (c) and a simulation of the results using a diffusion-decay  
 543 model (d) for an initial hole doping of  $10^{12}/\text{cm}^2$ .  
 544

545 The efficient generation of spin-valley current with remarkably large current densities reflects the  
 546 nearly ideal conversion of photogenerated excitons into a spin-valley imbalance. Still higher spin-



---

547 valley currents may be achievable in TMDC heterostructures by increasing the initial hole doping  
548 level to enable stronger optical pumping, as well as by improving the device quality to enhance the  
549 diffusivity. The long spin-valley lifetimes and diffusion lengths of valley-polarized holes in TMDC  
550 heterostructures hold promise for the generation, transport, and detection of spin-valley information  
551 and open exciting opportunities for the realization of future spintronic and valleytronic devices.  
552

### 553 **Concluding remarks**

554 Despite the rapid progress in the study of excited-states in van der Waals heterostructures  
555 summarized above, many outstanding questions remain in understanding charge transfer processes  
556 and the spin and valley relaxation dynamics.  
557

558 A complete picture of the underlying mechanism for the CT process in TMDC heterostructures  
559 remains elusive. First, the mechanisms developed to date do not account for the Coulombic  
560 interactions between electrons and holes, despite the existence of strongly bound excitons both in the  
561 TMDC monolayers<sup>8,97,98</sup> and in the heterostructures<sup>40</sup>. Though one can argue that the excitonic states  
562 are superpositions of the quasiparticle band states and, hence, are affected similarly, a quantitative  
563 picture in which excitonic correlations are taken into account remains a theoretical challenge. In this  
564 context, it would also be interesting to learn whether the dielectric environment of the heterostructure,  
565 which affects the excitonic interactions, also significantly influences the rate and efficiency of CT  
566 processes. In addition, the fact that changes in the dielectric screening of Coulombic interactions in  
567 TMDCs modify the quasiparticle band structure may provide a route to test the role of the Q and  $\Gamma$   
568 valleys in CT processes. Second, the time-domain probes of CT to date have been limited in their by  
569 the instrumental response function and have not generally yielded precise CT times. In addition,  
570 optical measurements, with their limited spatial resolution, average over moiré patterns formed  
571 between the two layers. This may lead to a washing out of predicted trends for CT times. Overcoming  
572 these limitations by improved temporal resolution and/or spatial resolution (such as through near-field  
573 techniques) would provide important experimental information to inform and test further theoretical  
574 models.  
575

576 Similarly many outstanding questions exist regarding spin and valley dynamics in TMDC  
577 heterostructures. Much more work is required to understand fully the intrinsic spin and valley  
578 dynamics in TMDC heterostructures and the dependence of the dynamics on the constituent TMDC  
579 materials, their relative crystallographic alignment, and their stacking order in multilayers. It remains,  
580 for example, unclear what factors define the ultimate limit for the spin-valley lifetime in TMDC  
581 heterostructures; also unknown is the role played by defects, edges, and grain boundaries, as well as  
582 possible effects from large-period moiré superlattices formed in TMDC heterostructures with small  
583 twist angles.  
584

586 **References**

587

- 588 1 Hunt, B. *et al.* Massive Dirac Fermions and Hofstadter Butterfly in a van der Waals  
589 Heterostructure. *Science* **340**, 1427-1430, (2013).
- 590 2 Ponomarenko, L. A. *et al.* Cloning of Dirac fermions in graphene superlattices. *Nature* **497**,  
591 594-597, (2013).
- 592 3 Dean, C. R. *et al.* Hofstadter's butterfly and the fractal quantum Hall effect in moire  
593 superlattices. *Nature* **497**, 598-602, (2013).
- 594 4 Spanton, E. M. *et al.* Observation of fractional Chern insulators in a van der Waals  
595 heterostructure. *Science* **360**, 62-66, (2018).
- 596 5 Cao, Y. *et al.* Unconventional superconductivity in magic-angle graphene superlattices. *Nature*  
597 **556**, 43-+, (2018).
- 598 6 Cao, Y. *et al.* Correlated insulator behaviour at half-filling in magic-angle graphene  
599 superlattices. *Nature* **556**, 80-+, (2018).
- 600 7 Chen, G. *et al.* Gate-Tunable Mott Insulator in Trilayer Graphene-Boron Nitride Moiré  
601 Superlattice. *Arxiv*, 1803.01985, (2018).
- 602 8 Chernikov, A. *et al.* Exciton Binding Energy and Nonhydrogenic Rydberg Series in Monolayer  
603 WS<sub>2</sub>. *Phys Rev Lett* **113**, (2014).
- 604 9 Ye, Z. L. *et al.* Probing excitonic dark states in single-layer tungsten disulphide. *Nature* **513**,  
605 214-218, (2014).
- 606 10 Xiao, D., Liu, G. B., Feng, W. X., Xu, X. D. & Yao, W. Coupled Spin and Valley Physics in  
607 Monolayers of MoS<sub>2</sub> and Other Group-VI Dichalcogenides. *Phys Rev Lett* **108**, (2012).
- 608 11 Xu, X. D., Yao, W., Xiao, D. & Heinz, T. F. Spin and pseudospins in layered transition metal  
609 dichalcogenides. *Nat Phys* **10**, 343-350, (2014).
- 610 12 Komsa, H. P. & Krasheninnikov, A. V. Electronic structures and optical properties of realistic  
611 transition metal dichalcogenide heterostructures from first principles. *Phys Rev B* **88**, (2013).
- 612 13 Gong, C. *et al.* Band alignment of two-dimensional transition metal dichalcogenides:  
613 Application in tunnel field effect transistors. *Appl Phys Lett* **103**, (2013).
- 614 14 Terrones, H., Lopez-Urias, F. & Terrones, M. Novel hetero-layered materials with tunable  
615 direct band gaps by sandwiching different metal disulfides and diselenides. *Sci Rep-Uk* **3**,  
616 (2013).
- 617 15 Stormer, H. L., Dingle, R., Gossard, A. C., Wiegmann, W. & Sturge, M. D. 2-Dimensional  
618 Electron-Gas at a Semiconductor-Semiconductor Interface. *Solid State Commun* **29**, 705-709,  
619 (1979).
- 620 16 Bellus, M. Z. *et al.* Type-I van der Waals heterostructure formed by MoS<sub>2</sub> and ReS<sub>2</sub>  
621 monolayers. *Nanoscale Horiz* **2**, 31-36, (2017).
- 622 17 Chiu, M. H. *et al.* Determination of band alignment in the single-layer MoS<sub>2</sub>/WSe<sub>2</sub>  
623 heterojunction. *Nat Commun* **6**, (2015).
- 624 18 Ozcelik, V. O., Azadani, J. G., Yang, C., Koester, S. J. & Low, T. Band alignment of two-  
625 dimensional semiconductors for designing heterostructures with momentum space matching.  
626 *Phys Rev B* **94**, (2016).
- 627 19 Hong, X. P. *et al.* Ultrafast charge transfer in atomically thin MoS<sub>2</sub>/WS<sub>2</sub> heterostructures. *Nat*  
628 *Nanotechnol* **9**, 682-686, (2014).
- 629 20 Wang, K. *et al.* Interlayer Coupling in Twisted WSe<sub>2</sub>/WS<sub>2</sub> Bilayer Heterostructures Revealed  
630 by Optical Spectroscopy. *Acs Nano* **10**, 6612-6622, (2016).
- 631 21 Kozawa, D. *et al.* Evidence for Fast Interlayer Energy Transfer in MoSe<sub>2</sub>/WS<sub>2</sub>  
632 Heterostructures. *Nano Lett* **16**, 4087-4093, (2016).
- 633 22 Zhang, C. X. *et al.* Systematic study of electronic structure and band alignment of monolayer  
634 transition metal dichalcogenides in Van der Waals heterostructures. *2d Mater* **4**, (2017).

635 23 Debbichi, L., Eriksson, O. & Lebegue, S. Electronic structure of two-dimensional transition  
636 metal dichalcogenide bilayers from ab initio theory. *Phys Rev B* **89**, (2014).

637 24 Zhang, J. F., Xie, W. Y., Zhao, J. J. & Zhang, S. B. Band alignment of two-dimensional lateral  
638 heterostructures. *2d Mater* **4**, (2017).

639 25 Qiu, D. Y., da Jornada, F. H. & Louie, S. G. Screening and many-body effects in two-  
640 dimensional crystals: Monolayer MoS<sub>2</sub>. *Phys Rev B* **93**, (2016).

641 26 Wilson, N. R. *et al.* Determination of band offsets, hybridization, and exciton binding in 2D  
642 semiconductor heterostructures. *Sci Adv* **3**, (2017).

643 27 Hill, H. M., Rigosi, A. F., Rim, K. T., Flynn, G. W. & Heinz, T. F. Band Alignment in MoS<sub>2</sub>/WS<sub>2</sub>  
644 Transition Metal Dichalcogenide Heterostructures Probed by Scanning Tunneling Microscopy  
645 and Spectroscopy. *Nano Lett* **16**, 4831-4837, (2016).

646 28 Ceballos, F., Bellus, M. Z., Chiu, H. Y. & Zhao, H. Ultrafast Charge Separation and Indirect  
647 Exciton Formation in a MoS<sub>2</sub>-MoSe<sub>2</sub> van der Waals Heterostructure. *Acs Nano* **8**, 12717-  
648 12724, (2014).

649 29 Heo, H. *et al.* Interlayer orientation-dependent light absorption and emission in monolayer  
650 semiconductor stacks. *Nat Commun* **6**, (2015).

651 30 Zhu, H. M. *et al.* Interfacial Charge Transfer Circumventing Momentum Mismatch at Two-  
652 Dimensional van der Waals Heterojunctions. *Nano Lett* **17**, 3591-3598, (2017).

653 31 Ji, Z. H. *et al.* Robust Stacking-Independent Ultrafast Charge Transfer in MoS<sub>2</sub>/WS<sub>2</sub> Bilayers.  
654 *Acs Nano* **11**, 12020-12026, (2017).

655 32 Chen, H. L. *et al.* Ultrafast formation of interlayer hot excitons in atomically thin MoS<sub>2</sub>/WS<sub>2</sub>  
656 heterostructures. *Nat Commun* **7**, (2016).

657 33 Ceballos, F., Ju, M. G., Lane, S. D., Zeng, X. C. & Zhao, H. Highly Efficient and Anomalous  
658 Charge Transfer in van der Waals Trilayer Semiconductors. *Nano Lett* **17**, 1623-1628, (2017).

659 34 Lee, C.-H. *et al.* Atomically thin p-n junctions with van der Waals heterointerfaces. *Nat*  
660 *Nanotechnol* **9**, 676, (2014).

661 35 Rigos, A. F., Hill, H. M., Li, Y. L., Chernikov, A. & Heinz, T. F. Probing Interlayer Interactions in  
662 Transition Metal Dichalcogenide Heterostructures by Optical Spectroscopy: MoS<sub>2</sub>/WS<sub>2</sub> and  
663 MoSe<sub>2</sub>/WSe<sub>2</sub>. *Nano Lett* **15**, 5033-5038, (2015).

664 36 Pan, S. D., Ceballos, F., Bellus, M. Z., Zereshki, P. & Zhao, H. Ultrafast charge transfer  
665 between MoTe<sub>2</sub> and MoS<sub>2</sub> monolayers. *2d Mater* **4**, (2017).

666 37 Xu, W. G. *et al.* Correlated fluorescence blinking in two-dimensional semiconductor  
667 heterostructures. *Nature* **541**, 62+, (2017).

668 38 Ceballos, F., Bellus, M. Z., Chiu, H. Y. & Zhao, H. Probing charge transfer excitons in a  
669 MoSe<sub>2</sub>-WS<sub>2</sub> van der Waals heterostructure. *Nanoscale* **7**, 17523-17528, (2015).

670 39 Li, Y. Y. *et al.* Ultrafast Interlayer Electron Transfer in Incommensurate Transition Metal  
671 Dichalcogenide Homobilayers. *Nano Lett* **17**, 6661-6666, (2017).

672 40 Rivera, P. *et al.* Observation of long-lived interlayer excitons in monolayer MoSe<sub>2</sub>-WSe<sub>2</sub>  
673 heterostructures. *Nat Commun* **6**, (2015).

674 41 Robert, C. *et al.* Exciton radiative lifetime in transition metal dichalcogenide monolayers. *Phys*  
675 *Rev B* **93**, (2016).

676 42 Xu, W. S. *et al.* Determining the Optimized Interlayer Separation Distance in Vertical Stacked  
677 2D WS<sub>2</sub>:hBN:MoS<sub>2</sub> Heterostructures for Exciton Energy Transfer. *Small* **14**, (2018).

678 43 Mak, K. F., Lee, C., Hone, J., Shan, J. & Heinz, T. F. Atomically Thin MoS<sub>2</sub>: A New Direct-Gap  
679 Semiconductor. *Phys Rev Lett* **105**, (2010).

680 44 Splendiani, A. *et al.* Emerging Photoluminescence in Monolayer MoS<sub>2</sub>. *Nano Lett* **10**, 1271-  
681 1275, (2010).

682 45 Zhu, X. Y. *et al.* Charge Transfer Excitons at van der Waals Interfaces. *J Am Chem Soc* **137**,  
683 8313-8320, (2015).

684 46 Wang, H. *et al.* The role of collective motion in the ultrafast charge transfer in van der Waals  
685 heterostructures. *Nat Commun* **7**, (2016).

686 47 Zhang, J. *et al.* Interlayer-State-Coupling Dependent Ultrafast Charge Transfer in MoS<sub>2</sub>/WS<sub>2</sub>  
687 Bilayers. *Adv Sci* **4**, (2017).

688 48 Long, R. & Prezhdo, O. V. Quantum Coherence Facilitates Efficient Charge Separation at a  
689 MoS<sub>2</sub>/MoSe<sub>2</sub> van der Waals Junction. *Nano Lett* **16**, 1996-2003, (2016).

690 49 Li, L. Q., Long, R. & Prezhdo, O. V. Charge Separation and Recombination in Two-  
691 Dimensional MoS<sub>2</sub>/WS<sub>2</sub>: Time-Domain ab Initio Modeling. *Chem Mater* **29**, 2466-2473, (2017).

692 50 Kang, J., Li, J. B., Li, S. S., Xia, J. B. & Wang, L. W. Electronic Structural Moire Pattern Effects  
693 on MoS<sub>2</sub>/MoSe<sub>2</sub> 2D Heterostructures. *Nano Lett* **13**, 5485-5490, (2013).

694 51 Tong, Q. J. *et al.* Topological mosaics in moire superlattices of van der Waals heterobilayers.  
695 *Nat Phys* **13**, 356-362, (2017).

696 52 Wang, Y., Wang, Z., Yao, W., Liu, G. B. & Yu, H. Y. Interlayer coupling in commensurate and  
697 incommensurate bilayer structures of transition-metal dichalcogenides. *Phys Rev B* **95**, (2017).

698 53 Zheng, Q. J. *et al.* Phonon-Assisted Ultrafast Charge Transfer at van der Waals  
699 Heterostructure Interface. *Nano Lett* **17**, 6435-6442, (2017).

700 54 Jin, C. H. *et al.* On Optical Dipole Moment and Radiative Recombination Lifetime of Excitons  
701 in WSe<sub>2</sub>. *Adv Funct Mater* **27**, (2017).

702 55 Zhang, X. X., You, Y. M., Zhao, S. Y. F. & Heinz, T. F. Experimental Evidence for Dark  
703 Excitons in Monolayer WSe<sub>2</sub>. *Phys Rev Lett* **115**, (2015).

704 56 Korn, T., Heydrich, S., Hirmer, M., Schmutzler, J. & Schuller, C. Low-temperature photocarrier  
705 dynamics in monolayer MoS<sub>2</sub>. *Appl Phys Lett* **99**, (2011).

706 57 Amani, M. *et al.* Near-unity photoluminescence quantum yield in MoS<sub>2</sub>. *Science* **350**, 1065-  
707 1068, (2015).

708 58 Moody, G. *et al.* Intrinsic homogeneous linewidth and broadening mechanisms of excitons in  
709 monolayer transition metal dichalcogenides. *Nat Commun* **6**, (2015).

710 59 Lagarde, D. *et al.* Carrier and Polarization Dynamics in Monolayer MoS<sub>2</sub>. *Phys Rev Lett* **112**,  
711 (2014).

712 60 Wang, Q. S. *et al.* Valley Carrier Dynamics in Mono layer Molybdenum Disulfide from Helicity-  
713 Resolved Ultrafast Pump-Probe Spectroscopy. *ACS Nano* **7**, 11087-11093, (2013).

714 61 Hao, K. *et al.* Direct measurement of exciton valley coherence in monolayer WSe<sub>2</sub>. *Nat Phys*  
715 **12**, 677+, (2016).

716 62 Mai, C. *et al.* Many-Body Effects in Valleytronics: Direct Measurement of Valley Lifetimes in  
717 Single-Layer MoS<sub>2</sub>. *Nano Lett* **14**, 202-206, (2014).

718 63 Zhu, C. R. *et al.* Exciton valley dynamics probed by Kerr rotation in WSe<sub>2</sub> monolayers. *Phys*  
719 *Rev B* **90**, (2014).

720 64 Mak, K. F., He, K. L., Shan, J. & Heinz, T. F. Control of valley polarization in monolayer MoS<sub>2</sub>  
721 by optical helicity. *Nat Nanotechnol* **7**, 494-498, (2012).

722 65 Zeng, H. L., Dai, J. F., Yao, W., Xiao, D. & Cui, X. D. Valley polarization in MoS<sub>2</sub> monolayers  
723 by optical pumping. *Nat Nanotechnol* **7**, 490-493, (2012).

724 66 Cao, T. *et al.* Valley-selective circular dichroism of monolayer molybdenum disulphide. *Nat*  
725 *Commun* **3**, (2012).

726 67 Glazov, M. M. *et al.* Exciton fine structure and spin decoherence in monolayers of transition  
727 metal dichalcogenides. *Phys Rev B* **89**, (2014).

728 68 Yu, T. & Wu, M. W. Valley depolarization due to intervalley and intravalley electron-hole  
729 exchange interactions in monolayer MoS<sub>2</sub>. *Phys Rev B* **89**, (2014).

730 69 Yu, H. Y., Liu, G. B., Gong, P., Xu, X. D. & Yao, W. Dirac cones and Dirac saddle points of  
731 bright excitons in monolayer transition metal dichalcogenides. *Nat Commun* **5**, (2014).

732 70 Maialle, M. Z., Silva, E. A. D. E. & Sham, L. J. Exciton Spin Dynamics in Quantum-Wells. *Phys*  
733 *Rev B* **47**, 15776-15788, (1993).

734 71 Hao, K. *et al.* Trion valley coherence in monolayer semiconductors. *2d Mater* **4**, (2017).

735 72 Volmer, F. *et al.* Intervalley dark trion states with spin lifetimes of 150 ns in WSe<sub>2</sub>. *Phys Rev B*  
736 **95**, (2017).

737 73 Plechinger, G. *et al.* Trion fine structure and coupled spin-valley dynamics in monolayer  
738 tungsten disulfide. *Nat Commun* **7**, (2016).

739 74 Zhang, X. X. *et al.* Magnetic brightening and control of dark excitons in monolayer WSe<sub>2</sub>. *Nat*  
740 *Nanotechnol* **12**, 883+, (2017).

741 75 Jiang, C. Y. *et al.* Microsecond dark-exciton valley polarization memory in two-dimensional  
742 heterostructures. *Nat Commun* **9**, (2018).  
743 76 You, Y. M. *et al.* Observation of biexcitons in monolayer WSe<sub>2</sub>. *Nat Phys* **11**, 477-U138,  
744 (2015).  
745 77 Chen, S., Goldstein, T., Taniguchi, T., Watanabe, K. & Yan, J. Coulomb-bound four- and five-  
746 particle valleytronic states in an atomically-thin semiconductor. *Arxiv*, 1802.10247, (2018).  
747 78 Dey, P. *et al.* Gate-Controlled Spin-Valley Locking of Resident Carriers in WSe<sub>2</sub> Monolayers.  
748 *Phys Rev Lett* **119**, (2017).  
749 79 Song, X. L., Xie, S. E., Kang, K., Park, J. & Sih, V. Long-Lived Hole Spin/Valley Polarization  
750 Probed by Kerr Rotation in Monolayer WSe<sub>2</sub>. *Nano Lett* **16**, 5010-5014, (2016).  
751 80 Hsu, W. T. *et al.* Optically initialized robust valley-polarized holes in monolayer WSe<sub>2</sub>. *Nat*  
752 *Commun* **6**, (2015).  
753 81 Yang, L. Y. *et al.* Long-lived nanosecond spin relaxation and spin coherence of electrons in  
754 monolayer MoS<sub>2</sub> and WS<sub>2</sub>. *Nat Phys* **11**, 830-U187, (2015).  
755 82 Fang, H. *et al.* Strong interlayer coupling in van der Waals heterostructures built from single-  
756 layer chalcogenides. *P Natl Acad Sci USA* **111**, 6198-6202, (2014).  
757 83 Nagler, P. *et al.* Interlayer exciton dynamics in a dichalcogenide monolayer heterostructure. *2d*  
758 *Mater* **4**, (2017).  
759 84 Rivera, P. *et al.* Valley-polarized exciton dynamics in a 2D semiconductor heterostructure.  
760 *Science* **351**, 688-691, (2016).  
761 85 Hsu, W. T. *et al.* Negative circular polarization emissions from WSe<sub>2</sub>/MoSe<sub>2</sub> commensurate  
762 heterobilayers. *Nat Commun* **9**, (2018).  
763 86 Hanbicki, A. T. *et al.* Double Indirect Interlayer Exciton in a MoSe<sub>2</sub>/WSe<sub>2</sub> van der Waals  
764 Heterostructure. *Arxiv*, 1802.05310, (2018).  
765 87 Ciarrocchi, A. *et al.* Control of interlayer excitons in two-dimensional van der Waals  
766 heterostructures. *Arxiv*, 1803.06405, (2018).  
767 88 Yu, H. Y., Wang, Y., Tong, Q. J., Xu, X. D. & Yao, W. Anomalous Light Cones and Valley  
768 Optical Selection Rules of Interlayer Excitons in Twisted Heterobilayers. *Phys Rev Lett* **115**,  
769 (2015).  
770 89 Yu, H. Y., Liu, B. L. & Yao, W. Brightened spin-triplet interlayer excitons and optical selection  
771 rules in van der Waals heterobilayers. 1803.01292, (2018).  
772 90 Miller, B. *et al.* Long-Lived Direct and Indirect Interlayer Excitons in van der Waals  
773 Heterostructures. *Nano Lett* **17**, 5229-5237, (2017).  
774 91 Kunstmann, J. *et al.* Momentum-space indirect interlayer excitons in transition-metal  
775 dichalcogenide van der Waals heterostructures. *Nat Phys*, (2018).  
776 92 Wu, F. C., Lovorn, T. & MacDonald, A. H. Theory of optical absorption by interlayer excitons in  
777 transition metal dichalcogenide heterobilayers. *Phys Rev B* **97**, (2018).  
778 93 Yu, H. Y., Liu, G. B., Tang, J. J., Xu, X. D. & Yao, W. Moire excitons: From programmable  
779 quantum emitter arrays to spin-orbit-coupled artificial lattices. *Sci Adv* **3**, (2017).  
780 i94 Kim, J. *et al.* Observation of ultralong valley lifetime in WSe<sub>2</sub>/MoS<sub>2</sub> heterostructures. *Sci Adv*  
781 **3**, (2017).  
782 95 Jin, C. H. *et al.* Imaging of Pure Spin-Valley Diffusion Current in WS<sub>2</sub>/WSe<sub>2</sub> Heterostructures.  
783 *Science*, in press, (2018).  
784 96 Carvalho, B. R. *et al.* Intervalley scattering by acoustic phonons in two-dimensional MoS<sub>2</sub>  
785 revealed by double-resonance Raman spectroscopy. *Nat Commun* **8**, (2017).  
786 97 Hill, H. M. *et al.* Observation of Excitonic Rydberg States in Monolayer MoS<sub>2</sub> and WS<sub>2</sub> by  
787 Photoluminescence Excitation Spectroscopy. *Nano Lett* **15**, 2992-2997, (2015).  
788 98 He, K. L. *et al.* Tightly Bound Excitons in Monolayer WSe<sub>2</sub>. *Phys Rev Lett* **113**, (2014).  
789  
790

---

791 **Acknowledgements**

792 E.Y.M. acknowledge support from the Department of Energy, Office of Science, Basic Energy  
793 Sciences, Materials Sciences and Engineering Division, under Contract DE-AC02-76SF00515; T. F.H.  
794 acknowledges support from the AMOS program, Chemical Sciences, Geosciences, and Biosciences  
795 Division, Basic Energy Sciences, US Department of Energy under Contract DE-AC02-76-SF00515  
796 and from the Betty and Gordon Moore Foundation's EPIQS Initiative through Grant No. GBMF4545.  
797 O.K. acknowledges the support of the Rothschild Fellowship of Yad Hanadiv Fund, Israel, and of the  
798 Viterbi Fellowship of the Andrew and Erna Viterbi Department of Electrical Engineering, Technion,  
799 Israel. F.W. and E.C.R. acknowledge support from the Director, Office of Science, Office of Basic  
800 Energy Sciences, Materials Sciences and Engineering Division of the U.S. Department of Energy  
801 under Contract No. DE-AC02-05-CH11231 (van der Waals heterostructures program, KCWF16). C.J.  
802 acknowledges the support from the National Science Foundation EFRI program (EFMA-1542741).

803

804